

UC Irvine

UC Irvine Previously Published Works

Title

On the effects of the Hadley circulation and westerly equatorial flow on planetary-wave reflection

Permalink

<https://escholarship.org/uc/item/2z76v3sq>

Journal

Quarterly Journal of the Royal Meteorological Society, 126(569)

ISSN

0035-9009

Authors

Magnusdottir, G
Walker, CC

Publication Date

2000

DOI

10.1256/smsqj.56906

Copyright Information

This work is made available under the terms of a Creative Commons Attribution License, available at

<https://creativecommons.org/licenses/by/4.0/>

Peer reviewed

On the effects of the Hadley circulation and westerly equatorial flow on planetary-wave reflection

By GUDRUN MAGNUSDOTTIR* and CHRISTOPHER C. WALKER

University of California, Irvine, USA

(Received 24 September 1999; revised 12 June 2000)

SUMMARY

The nonlinear behaviour of quasi-stationary planetary waves that are excited by mid-latitude orographic forcing is considered in a global shallow-water model taken to represent the upper troposphere. The waves propagate toward low latitudes where the background flow is normally weak and the waves are therefore likely to break. Nonlinear pseudomomentum conservation relations are used to quantify the absorption–reflection behaviour of the wave-breaking region. Two different flow scenarios are represented: (i) initial states without a representation of the Hadley circulation, but where the axisymmetric equatorial background flow changes from being weak and easterly to moderate westerly; (ii) initial states that include a representation of the Hadley circulation and that have weak equatorial easterlies.

Based on linear arguments, both (i) and (ii) are expected to influence the progression of the wave train. The nonlinear behaviour in the presence of low-latitude westerly background flows is different from linear predictions. For large-amplitude forcing, wave breaking takes place even though there is no zero-wind line in the initial state, and the cross-equatorial wave propagation that took place for small-amplitude forcing is stopped before it can reach the equator. Nonlinear reflection is found to take place back into the hemisphere of origin but not across to the other hemisphere.

In the presence of a Hadley circulation representative of winter conditions, the nonlinear reflection takes longer to get established, i.e. it requires more forcing, but a reflected wave train is still present in the numerical simulations, both for a longitudinally symmetric forcing and for the more realistic case of an isolated forcing. A summer Hadley circulation allows wave activity to get to the winter hemisphere. As the forcing is increased, wave breaking occurs and eventually nonlinear reflection.

KEYWORDS: Hadley circulation Nonlinear reflection Planetary waves Westerly equatorial flow

1. INTRODUCTION

Observations have shown that the wintertime subtropical upper troposphere is a region of strong Rossby wave breaking. This gets manifested, for example, in maps of potential vorticity (PV) on upper-tropospheric isentropic surfaces, which show the PV field to be well mixed at subtropical latitudes. As quasi-stationary Rossby waves propagate toward low latitudes, where the background flow is weak, the linear balance of terms breaks down and, given small enough dissipation, the waves must break. Winter is also the season when the Hadley circulation is at its strongest.

Previous studies have addressed the possibility of nonlinear reflection from Rossby wave-breaking regions. Killworth and McIntyre (1985, hereafter KM) emphasized conditions in the stratospheric surf zone since they considered wave trains that were monochromatic in longitudinal wave number, a condition that is not typically seen in tropospheric observations. Assuming a balanced two-dimensional flow, they were able to bound the momentum flux into the wave-breaking region by using a finite-amplitude, wave-activity conservation relation. Brunet and Haynes (1996, hereafter BH) used a shallow-water equation (SWE) model to simulate conditions in the upper troposphere. In the case of flow that is not balanced (such as the SWE), no theoretical bound can be put on the absorption of wave activity in the critical layer. Still, the numerical experiments can be analysed in terms of finite-amplitude, wave-activity diagnostics. BH found strong evidence in their numerical experiments that an isolated wave train was reflected toward mid latitudes as the amplitude of forcing was increased. Magnusdottir and Haynes

* Corresponding author: Department of Earth System Science, 220 Rowland Hall, University of California, Irvine, CA 92697-3100, USA. e-mail: gudrun@uci.edu

(1999, hereafter MH99) generalized these results to fully three-dimensional, primitive-equation flows. They also addressed the effects of thermal damping and horizontal resolution on these findings. They found that thermal damping did not inhibit the nonlinear reflection behaviour. However, the diffusion of the smallest horizontal scales, that necessarily must be included for numerical stability, prevented nonlinear reflection when the horizontal resolution was reduced to T21. That this was due to the diffusion and not to the decrease in resolution itself was verified by running the model at higher horizontal resolution while using the diffusion of smallest horizontal scales required for numerical stability at T21. Nonlinear reflection was completely prevented, even for very large-amplitude forcing, at model resolution of T42 with this value of diffusion (MH99, section 7).

A study by Waugh *et al.* (1994) considered the effects of varying the axisymmetric, low-latitude, longitudinal velocity field on the propagation and breaking of an isolated quasi-stationary wave train in a global nondivergent barotropic model, using contour dynamics. As they went into the nonlinear regime, applying stronger forcing, they found wave breaking in the tropics even in the absence of a zero-wind line. The wave-breaking region impeded any further propagation of the wave train into the opposite hemisphere. Nonlinear reflection out of the wave-breaking region was not the subject of their study although they noted some evidence for reflected waves.

Rossby wave propagation is the primary mechanism by which longitudinal variations of the time-mean flow get established. The fate of Rossby waves at critical lines is certainly important for the structure of the mid-latitude wave field. Even though recent studies (e.g. Branstator 1992) have suggested strong interactions between transient eddies and low-frequency variations, it appears that there is still much to be gained from simple models that treat the low-frequency variations in isolation, while still including nonlinear effects. Here we extend this line of investigation further in two ways using a SWE model. Firstly, we examine the wave-breaking and reflecting behaviour of quasi-stationary Rossby waves when the equatorial background flow changes from an easterly to a westerly direction. Webster and Holton (1982) suggested that regions of westerly flow, which are observed in the eastern Pacific and Atlantic, might act as 'ducts' allowing cross-equatorial wave propagation. Hoskins and Ambrizzi (1993) suggest, on the basis of a linear study, that any cross-equatorial propagation is likely to be weak. In the context of nonlinear studies, such as the one reported on here, the cross-equatorial propagation may be inhibited if the westerlies are only weak (as is observed) and therefore wave breaking can take place as a result of finite wave amplitudes. Nonlinear reflection may well occur in such cases, although there may also be nonlinear radiation into the opposite hemisphere if there are neighbouring westerlies there to support wave propagation. Here, we expand on the study by Waugh *et al.* (1994) in that we shall concentrate on studying any nonlinear reflection (or re-radiation) occurring as a result of finite-amplitude forcing.

Secondly, we examine the effect of the Hadley circulation on nonlinear reflection. The winter Hadley case is more relevant for studying the reflective properties of the flow, since it is in winter that observations (e.g. Hsu *et al.* 1990; Kiladis and Weickman 1992) have shown there to be active wave breaking at upper levels in the subtropics. In the winter case, not only will the meridional component of the velocity tend to oppose the propagation of stationary Rossby waves to low latitudes (Watterson and Schneider 1987), but the Hadley circulation may act to maintain the low-latitude gradients of PV, thus violating one of the key assumptions required for the theoretical KM bound and hence inhibiting reflection. Non-conservative effects associated with the Hadley cell may also inhibit reflection by acting directly to dissipate wave activity at low latitudes.

Some of the nonlinear effects of the winter Hadley circulation have been considered by Held and Phillips (1990), who studied the interactions of a stationary Rossby wave (of longitudinal wave number three) with a zonally symmetric Hadley circulation in a single-layer model. Their main emphasis was on the zonal-mean momentum budget, using the stationary wave as a substitute for the full spectrum of Rossby waves generated in mid latitudes, to examine the maintenance of the subtropical jet. The results of their numerical experiments seem to indicate that wave absorption could be maintained, since a breaking event is followed by the regeneration of absolute vorticity in the wave-breaking region. However, the focus of their study was not on whether nonlinear reflection might be possible. Here we expand on their work, both in generalizing some of the assumptions made and in taking advantage of the finite-amplitude, wave-activity diagnostics in analysing numerical results. We find strong evidence of nonlinear reflection both for wave number three waves and for an isolated wave train.

Independent work by Esler *et al.* (2000, hereafter EPP) considers the effects of the winter Hadley circulation on planetary wave propagation and reflection in a SWE model. Since one part of the present study is similar to parts of EPP, we shall compare our numerical simulations with EPP in section 4, and thereby attempt to complement their numerical simulations. Of course, our study has different parameter settings. EPP conclude that the Hadley circulation delays and weakens the nonlinear reflection of a periodic wave train, and prevents the nonlinear reflection of an isolated wave train. Thus they reach different conclusions from quite similar experiments.

The plan of the paper is as follows. In section 2 we introduce the set-up for the numerical experiments as well as the diagnostics that are used. In sections 3, 4 and 5 we present numerical results. The effects of varying the zonal background flow on nonlinear wave reflection is analysed in section 3. In section 4, we consider the effects of a winter Hadley circulation on the propagation, breaking and nonlinear reflection of planetary waves. In section 5, we briefly consider the effects of a summer Hadley circulation. Section 6 contains a summary and discussion of the results.

2. SOME PRELIMINARIES

(a) Numerical model, parameter settings and forcing

The SWEs on the sphere are given by the following equations for momentum and mass continuity:

$$\frac{\partial u}{\partial t} - \zeta v + \frac{\partial}{a \cos \phi \partial \lambda} \{g(\sigma + h) + \frac{1}{2}(u^2 + v^2)\} = -\kappa_m \bar{u}, \quad (1)$$

$$\frac{\partial v}{\partial t} + \zeta u + \frac{\partial}{a \partial \phi} \{g(\sigma + h) + \frac{1}{2}(u^2 + v^2)\} = -\kappa_m \bar{v}, \quad (2)$$

$$\frac{\partial \sigma}{\partial t} + \frac{\partial(\sigma u)}{a \cos \phi \partial \lambda} + \frac{\partial(\sigma v \cos \phi)}{a \cos \phi \partial \phi} = -\tau^{-1}(\bar{\sigma} - \sigma_E), \quad (3)$$

where u and v are components of horizontal velocity in the longitudinal (λ) and latitudinal (ϕ) directions, respectively, a is the radius of the earth, $\zeta = 2\Omega \sin \phi + \frac{\partial v}{a \cos \phi \partial \lambda} - \frac{\partial(u \cos \phi)}{a \cos \phi \partial \phi}$ is the absolute vorticity, σ is the deviation of the layer thickness from the globally averaged thickness of 2 km, h is the deviation of the lower surface away from being perfectly spherical, σ_E is a specified layer thickness, and g is the gravitational acceleration. The overbar denotes averaging in longitude. In what follows, $P = \zeta/\sigma$ is PV, the momentum relaxation time-scale is κ_m^{-1} , and the thermal relaxation time-scale

is τ . For the simulations in section 3 (before introducing the Hadley circulation), we neglect the terms on the right-hand side in (1)–(3) and use the same form of the equations as BH. When we force a zonally symmetric Hadley circulation in section 4, we employ both Rayleigh friction and a zonally symmetric mass source/sink.

Rayleigh friction with a constant damping rate of $\kappa_m = 10 \text{ day}^{-1}$ is applied to the zonally averaged momentum on the right-hand side of (1) and (2). A zonally symmetric mass source/sink term, representing thermal forcing, is included on the right-hand side of the continuity equation (3). The mass forcing term is a relaxation towards the specified layer thickness $\sigma_E(\phi)$, with time constant $\tau(\phi)$, and is intended to simulate the effects of differential solar heating and radiative cooling. The mass source, which is centred around a latitude of maximum heating (here 10°S and 10°N , for northern winter and summer conditions, respectively), represents inflow of mass into the layer due to convection. The mass sink is present poleward of the mass source, and it represents mass transported out of the layer as a result of radiative cooling. (σ_E is shown by the dashed curve in Fig. 4(c) as a function of latitude for winter conditions.) The thermal-damping time-scale, $\tau(\phi)$, varies from a minimum of one day at the latitude of maximum heating to five days at a distance of 10° latitude away from the maximum mass source, and it increases rapidly to a value of 11 days in the far field.

The numerical model is a SWE version of the Reading spectral model (Hoskins and Simmons 1975). It is a spectral model that integrates the SWE in vorticity/divergence form. It was run both at T42 and T106 resolution with ∇^6 hyperdiffusion added to the vorticity, divergence, and thickness tendency equations with a decay rate of 8.3 day^{-1} for the smallest scales. The results displayed in the figures were obtained at T106.

Topography is included in the model through the term h , and that is one way in which we excite quasi-stationary Rossby waves. The other way to excite Rossby waves is by including a vorticity source. We use the same topography as in MH99: an isolated Gaussian mountain centred at 45°N , 0°W with a half radius of 1066 km, and a mountain with a zonal wave-number-three structure and the same latitudinal structure as the isolated forcing. The amplitude of the forcing is increased gradually over the first four days of integration. The amplitude of forcing is scaled in terms of 2 km, which is the globally averaged thickness. Each experiment is run for 50 days and the results are shown for the first 30 days.

Many previous studies have used a single-layer model to simulate the upper-tropospheric circulation. The choice of the mean layer thickness depends on the particular application of the study. If the focus is on low-latitude behaviour, such that tropical heating is important in forcing the flow, typical values range from 100 m (such as Held and Phillips 1990) to 500 m. (See Fulton and Schubert (1985) for a discussion of the tropical tropospheric response to organized convection and the dominance of baroclinic modes ranging in depth from 100 to 500 m.) On the other hand, studies that concentrate on the equivalent barotropic mid-latitude Rossby wave behaviour use a mean thickness of 7–9 km. Here, we chose an intermediate value. Following Webster and Holton (1982), we chose a mean thickness of 2 km, which is between the values of 100 m used by Held and Phillips (1990) and 4 km chosen by BH.

(b) Diagnostics

The advantages of using wave-activity fluxes to diagnose wave behaviour in numerical simulations and in observations have been demonstrated, e.g. by Edmon *et al.* (1980) and Plumb (1985). For problems in which wave amplitudes are not small there is particular advantage in using wave activities for which there is a finite-amplitude

conservation relation, i.e. there are, in conservative flows, no sources or sinks of wave activity associated with nonlinearities in the flow. Wave activities conserved at finite amplitude that are expressed in terms of Eulerian quantities only (without any reference to particle displacements) are particularly useful for practical applications. For using such wave activities the flow must be split into a predetermined basic-state part, denoted by $(\cdot)_0$, and a disturbance part, denoted by $(\cdot)_e$, which is simply the deviation from the basic state such that $(\cdot) = (\cdot)_0 + (\cdot)_e$. The basic state must be a self-consistent solution of the equations of motion and it must have a symmetry property. We shall use basic states that are independent of longitude; the resulting wave activity is usually referred to as ‘pseudomomentum’. Two additional requirements are placed on the basic state. In addition to being zonally symmetric, for practical applications it must also have a monotonic latitudinal gradient of PV. Instead of requiring Lagrangian variables, the function m_0 , where

$$m_0\{P_0(\phi)\} = \int_0^\phi \sigma_0(\tilde{\phi}) a \cos \tilde{\phi} d\tilde{\phi}, \tag{4}$$

must be a monotonic function of latitude. According to (4), $m_0\{P_0(\phi)\}$ is the mass measured from the equator to that latitude ϕ in the basic state that has a PV value of P_0 . For ease of interpretation and for comparison with two-dimensional balanced flow, it is easiest to think of m_0 as being a measure of position in the latitudinal direction based on the basic-state PV field. The third requirement of the basic state is that it be defined such that the phenomenon of interest is appropriately highlighted. See Magnusdottir and Haynes (1996) for a discussion of the choice of basic states that highlight the development of baroclinic-wave life cycles.

The conservation of pseudomomentum may be expressed as

$$\frac{\partial A}{\partial t} + \nabla \cdot \mathbf{F} = \frac{\partial A}{\partial t} + \frac{1}{a \cos \phi} \frac{\partial F^{(\lambda)}}{\partial \lambda} + \frac{1}{a \cos \phi} \frac{\partial (F^{(\phi)} \cos \phi)}{\partial \phi} = S, \tag{5}$$

where, following Haynes (1988), A , the pseudomomentum density, is given by

$$A = -\sigma_e u_e \cos \phi + \sigma \int_0^{P_e} \{m_0(P_0 + \tilde{P}) - m_0(P_0)\} d\tilde{P}. \tag{6}$$

Thus, according to the definition of m_0 above, the integral in (6) represents a measure of the excursion of fluid particles in the disturbed flow away from the basic state. For small Rossby number flows, it can be shown that the integral term in (6), the expression for pseudomomentum density, dominates the first term. This second term expresses the wave activity arising from PV rearrangement in the flow and is comparable to KM’s expression for pseudomomentum density in the case of two-dimensional vortex dynamics. The KM bound on the time-integrated wave-activity flux into the wave-breaking region depends on bounding the wave activity by a function involving the disturbance PV and hence particle displacements. The presence of the first term in (6) means that this is not possible for the SWE although, for flows that are close to being balanced, the expectation is that a bound is likely to hold in practice. This was indeed confirmed by BH, and by MH99 for the primitive-equation case.

Following BH, components of the pseudomomentum flux are given by

$$F^{(\lambda)} = uA - \frac{1}{2}\sigma_0(u_e^2 - v_e^2) \cos \phi + \frac{1}{2}g\sigma_e^2 \cos \phi + \frac{1}{a} \frac{\partial}{\partial \phi} \Psi, \tag{7}$$

$$F^{(\phi)} = vA - \sigma_0 v_e u_e \cos \phi - \frac{\partial}{a \cos \phi \partial \lambda} \Psi, \tag{8}$$

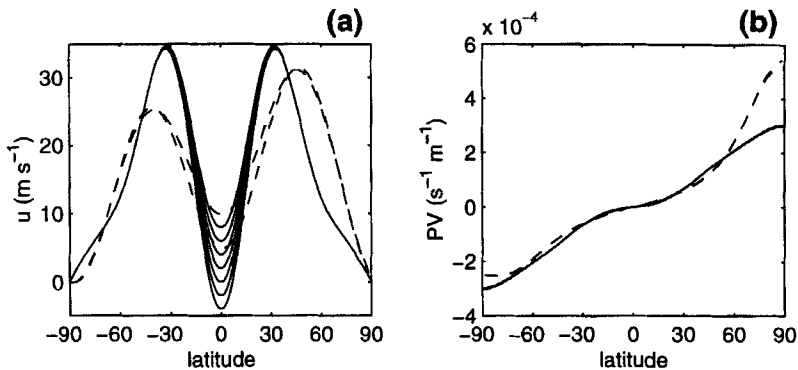


Figure 1. Initial states for the nearly inviscid experiments. (a) The axisymmetric longitudinal wind profiles (in m s^{-1}) as functions of latitude. The solid curves correspond to variations of the Held profile, the dashed curves to the Waugh *et al.* westerly profiles. (b) The corresponding initial potential vorticity profiles ($\text{s}^{-1} \text{m}^{-1}$) as functions of latitude.

where $\Psi = -\frac{1}{2}u_e\psi_e\sigma_0 \cos \phi$ and ψ is the stream function for the nondivergent part of the flow. The terms involving Ψ in (7) and (8) remove phase variations of the flux on the scale of the wavelength of the stationary Rossby waves that are studied here. This method of removing phase variations of the flux (first used by Plumb (1985)) has also proved to be valuable for primitive-equation flows (MH99). See Vanneste and Shepherd (1998) for a method of deriving wave-activity relations that bypasses the need for any such correction.

When the only non-conservative process, aside from the wave forcing itself, is the small-scale diffusion that is added for numerical stability, the non-conservative term S in (5) is negligible away from the area of forcing. This is the case that will be studied in the next section.

3. THE EFFECT OF VARYING THE LOW-LATITUDE ZONAL FLOW ON NONLINEAR REFLECTION

The numerical model was initialized with the different zonal flow profiles shown in Fig. 1(a). The solid curves in Fig. 1(a) are slight variations on the Held (1985) profile (also used by BH and MH99). The equatorial zonal wind speed has the following values for these different experiments: -4 , -2 , 0 , 2 , 4 , 6 and 8 m s^{-1} . The dashed curves in Fig. 1(a) represent the two equatorial westerly profiles used by Waugh *et al.* (1994), which we considered for comparison. The initial height field was chosen so that it was in gradient wind balance with the wind field. The resulting initial PV fields are shown in Fig. 1(b). We integrated (1)–(3), setting $\kappa_m = 0$ and $\tau^{-1} = 0$.

Previous studies (e.g. Grose and Hoskins 1979) have shown that the response to a mid-latitude isolated forcing takes the form of two eastward propagating wave trains, where one propagates to high and the other to low latitudes. Consistent with the results of BH, we find that if the forcing is of small amplitude and the equatorial background flow is easterly, the wave train propagating to low latitudes terminates before reaching the zero-wind line. According to (5), this means that the small-scale diffusion (the only non-conservative process away from the forcing) is enough to balance the wave-activity flux into the critical layer, which acts as an absorber. As the forcing is increased, wave breaking takes place, and it occurs earlier the stronger the forcing. As wave breaking

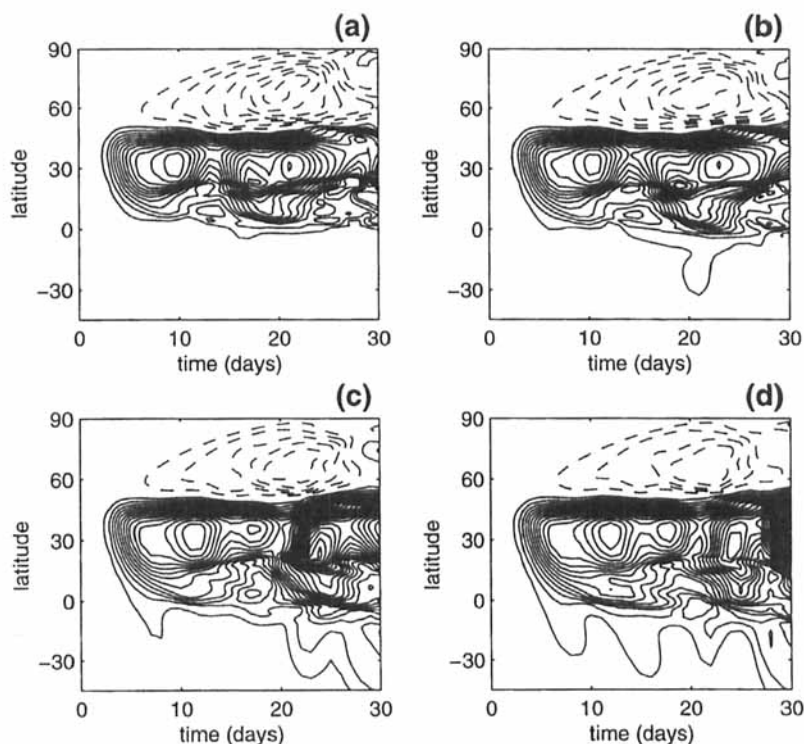


Figure 2. Time evolution (days) of the longitudinal average of the normalized southward pseudomomentum flux, shown as contour diagrams in the time–latitude plane for isolated forcing of amplitude 0.2 and four different initial wind profiles. The equatorial background flow is: (a) -4 m s^{-1} , (b) zero, (c) 4 m s^{-1} , (d) 6 m s^{-1} . Dashed contours are negative.

continues there comes a point when the wave-breaking region saturates, and in order to satisfy (5) there is a return flux out of the region.

Consistent with earlier studies (e.g. Hoskins *et al.* 1977), we find that at small amplitude and for a westerly equatorial background flow, the wave train propagates freely into the other hemisphere. As the equatorial background flow becomes more westerly, for the same small-amplitude forcing, more wave activity gets into the opposite hemisphere as a result of cross-equatorial wave propagation. This has been quantified for the initial states depicted in Fig. 1. Consistent with Waugh *et al.* (1994), as the forcing becomes stronger the propagation is hindered, and wave breaking occurs in all cases including those that have positive equatorial flow. Figure 2 shows contour diagrams of the zonally averaged, southward pseudomomentum flux as a function of time and latitude for the strong-amplitude case of 0.2, and for basic states that have several different equatorial wind speeds. Figure 2(a) is for the case that has an equatorial windspeed of -4 m s^{-1} , and it is therefore similar to the results shown by BH. The pseudomomentum flux builds up to a maximum around 30°N at around days 9 to 10. Thereafter the flux decreases sharply, which signals the onset of nonlinear reflection from the wave-breaking region. When the equatorial wind speed is zero in Fig. 2(b) there is again a sharp decrease in flux, but now it occurs somewhat later, on day 11. Even for the positive equatorial flows of 4 and 6 m s^{-1} , depicted in Fig. 2(c) and (d), respectively, there is a clear reduction in flux indicative of reflection, occurring later the greater the equatorial westerlies of the initial state. Thus, the more westerly the

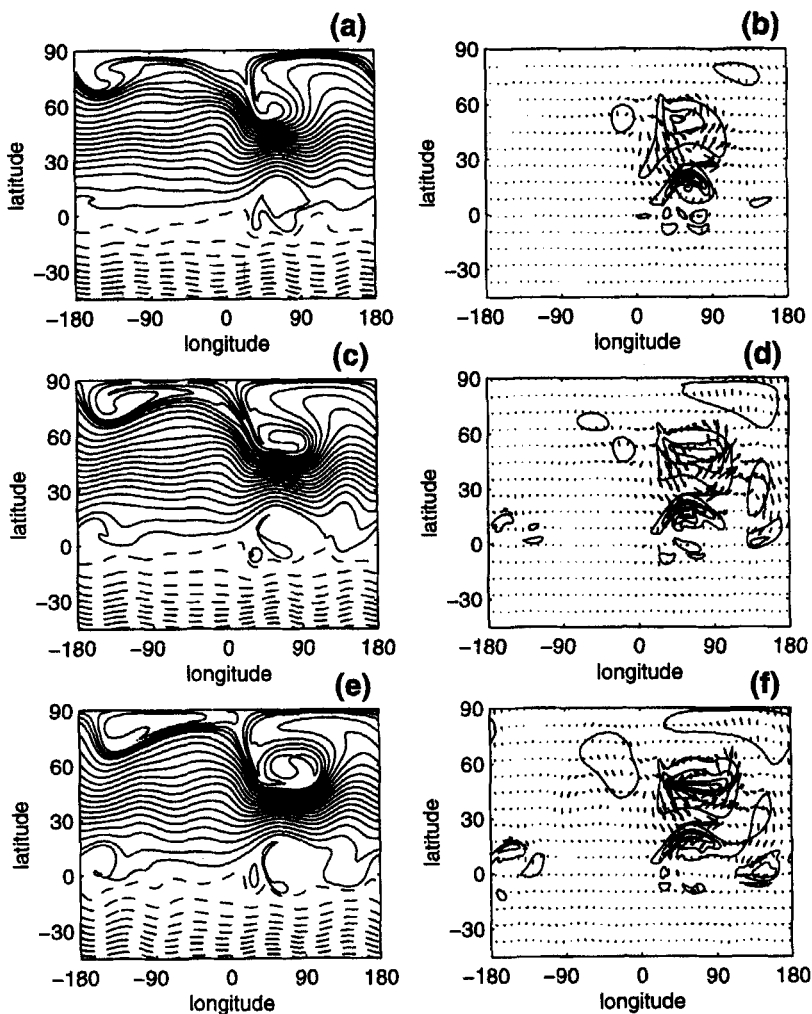


Figure 3. Potential vorticity, PV, and pseudomomentum density and flux in the latitude–longitude plane for an isolated mid-latitude forcing of amplitude 0.2 in an initial state that has equatorial background winds of 6 m s^{-1} . (a) PV on day 18; (b) pseudomomentum density and flux on day 18; (c) PV on day 22; (d) pseudomomentum density and flux on day 22; (e) PV on day 26; (f) pseudomomentum density and flux on day 26. Dashed contours are negative.

background flow field, the longer it takes (for the same forcing amplitude) to saturate the wave-breaking region. We also examined basic states with westerly equatorial wind speeds of 8 and 10 m s^{-1} and found the same behaviour.

Let us focus on the case that has equatorial flow of 6 m s^{-1} in the initial state and is forced by a forcing amplitude of 0.2. This is the case depicted in Fig. 2(d). Figure 3 shows snapshots of the PV field as well as pseudomomentum density and flux, 18, 22 and 26 days into the simulation. By day 18 there has been considerable PV rearrangement at low latitudes, centred at 60°E , shown in Fig. 3(a). The pseudomomentum density at this time (in Fig. 3(b)) shows the accumulation of wave activity at low latitudes, primarily in the northern hemisphere, but with weak maxima just south of the equator. The weak southern hemispheric signatures are not seen in the wave-activity density field when the initial state has equatorial easterlies. The pseudomomentum flux

in Fig. 3(b) is directed into the wave-breaking region and clearly back out towards the north-east. This is the familiar signature of nonlinear reflection shown in BH and MH99 for easterly equatorial flow. Four-days later in Fig. 3(c), the PV field shows a secondary region of rearrangement, centred about 150°E . The pseudomomentum flux at this time, in Fig. 3(d), shows that the reflected wave train has curved equatorward, and the downstream perturbed region is a result of this reflected wave train leading to a build up of wave activity at low latitudes. Finally, by day 26, there is evidence of multiple reflection, with the wave train reflected in the neighbourhoods of 60°E and 150°E , with a third region at 120°W where the wave train is turning equatorward again in Fig. 3(f). When we initialized the model with the Waugh *et al.* (1994) equatorial westerly initial states (dashed curves in Fig. 1) the reflection was of similar character, so that it appears to be independent of the details of the flow away from the wave-breaking region.

It is interesting that the nonlinear reflection always appears to be directed into the hemisphere of forcing, with no clear evidence of cross-equatorial re-radiation (or nonlinear reflection), although late in the simulation in Fig. 2(d) there appears to be a burst of flux across the equator. It is difficult to establish unequivocally that there is no reflection across the equator, since the linear response has wave propagation across the equator. Any reflected wave train in the nonlinear response would be considerably weaker, and the nonlinear signature as expressed in a difference field between the nonlinear and linear responses would be swamped by the linear field. When we inserted vorticity forcing of a similar spatial structure to that in the wave-breaking region, we found that by far the strongest response was into the northern hemisphere with a substantially weaker response to the south.

4. WAVE BREAKING AND NONLINEAR REFLECTION IN THE PRESENCE OF A WINTER HADLEY CIRCULATION

A Hadley circulation was forced by applying Rayleigh friction and Newtonian cooling as described in section 2(a). We integrated the model (with $h = 0$) to steady state, and the resulting zonally symmetric state had a Hadley circulation with a maximum meridional wind speed of 2.5 m s^{-1} . We shall call this initial state, which is depicted in Fig. 4, the Hadley state. Figure 4(a) shows that the resulting zonal jet has maximum winds of 47 m s^{-1} at 33°N ; Fig. 4(b) shows the meridional velocity, Fig. 4(c) the perturbation thickness and Fig. 4(d) the resulting PV profile. The dashed curve in Fig. 4(c) shows the σ_E field, towards which the thickness field is relaxed in (3).

In order to determine the effect of the Hadley circulation on Rossby wave behaviour, we also integrated (1)–(3) without any mass sources or sinks, but we included Rayleigh friction. In (1) we forced the zonally averaged zonal flow back to the Hadley-state zonal flow. We shall call the initial state for this second set of experiments the no-Hadley state. To obtain a no-Hadley state that is as close as possible to the above Hadley state, we take the Hadley velocity field and set the meridional component to zero, but keep the zonal component the same as that shown in Fig. 4(a). We then determine the thickness field such that the no-Hadley state is in gradient wind balance. This thickness field is quite close to the Hadley-state thickness field and, in fact, the resulting PV fields for both cases are shown in Fig. 4(d). The difference between the two PV fields is three orders of magnitude smaller than each field, and the two PV fields are indistinguishable in the figure. Note that the no-Hadley initial state satisfies the requirements for a basic state that we listed in section 2(b), and it is unforced. This is the basic state that we use for calculating pseudomomentum diagnostics for both sets of experiments. The term S in

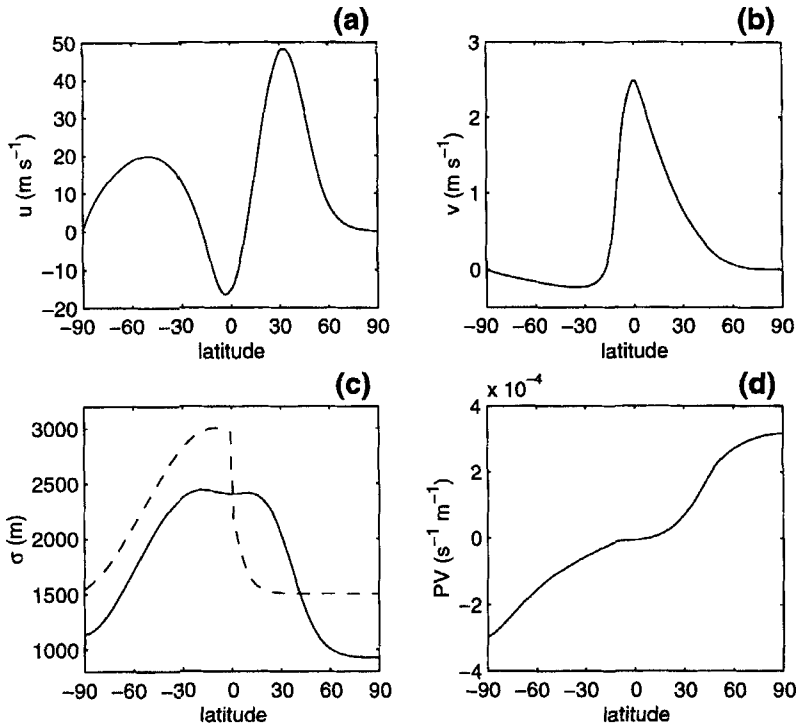


Figure 4. The initial state for the simulations that include a representation of the winter Hadley circulation; all fields depend only on latitude. (a) Zonal wind (m s^{-1}); (b) meridional wind (m s^{-1}); (c) the thickness field (m, solid curve) and the thickness field towards which the thickness is relaxed (the mass forcing, dashed curve); (d) the resulting potential vorticity field ($\text{s}^{-1} \text{m}^{-1}$).

(5) is, therefore, entirely due to non-conservative effects acting on the waves, as well as the wave-source term.

In the EPP study, the meridional wind due to the Hadley circulation is positive everywhere and has a maximum speed of 1.7 m s^{-1} , which is weaker than the maximum meridional wind speed in the current study. Even though these are highly idealized experiments, it should be noted that observations show that the upper-tropospheric winter Hadley circulation (in the zonal average) has a winter mean wind speed in excess of 2.5 m s^{-1} (e.g. Min and Schubert 1997). The steady states of both the current study and that of EPP include a zonal jet that has a maximum wind speed of 47 m s^{-1} , which is considerably stronger than the observed winter mean jet of 40 m s^{-1} .

(a) *Longitudinally periodic forcing*

The topographic forcing is of wave number three in longitude. Several different amplitudes of forcing were considered, ranging from a small-amplitude case of 0.005, which showed no evidence of low-latitude wave breaking for either the Hadley or the no-Hadley case, to the large amplitude case of 0.2. As we got into the nonlinear regime, several differences became apparent between the Hadley and no-Hadley experiments. First and foremost is the difference in the low-latitude wave-breaking region itself, with the Hadley case displaying continuing gradients of PV even late in the integration, whereas the no-Hadley case is close to being well-mixed through small-scale hyperdiffusion. This is consistent with the findings of EPP in a slightly different parameter regime.

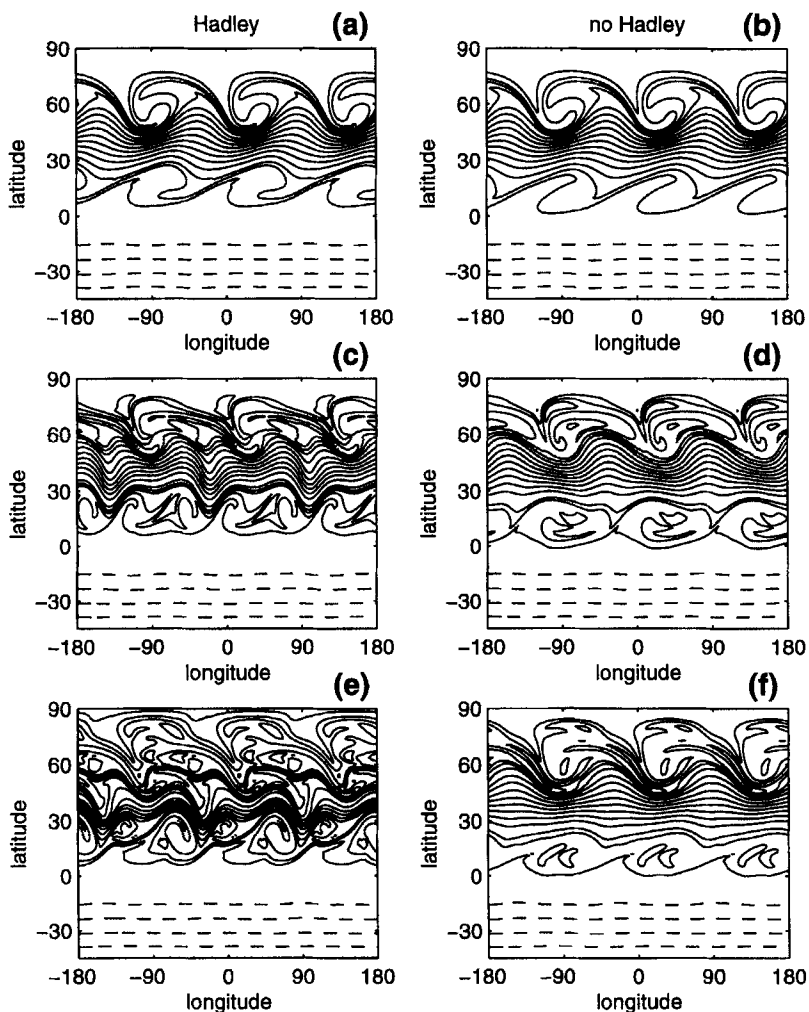


Figure 5. Instantaneous plots of potential vorticity in the latitude–longitude plane for wave-number-three forcing of amplitude 0.1. The left-hand panels correspond to cases where there is an active Hadley circulation; the right-hand panels correspond to cases that have no mass sources or sinks but are otherwise the same: (a) and (b) day 8; (c) and (d) day 16; (e) and (f) day 24. Dashed contours are negative.

(Note that the only other non-conservative process in the no-Hadley case is Rayleigh friction that only acts on the zonally symmetric part of the flow.) In the Hadley case, where the mass source is active on very short time-scales in low latitudes, there is a continuing source of PV throughout the integration. This means that, even though there is continual wave breaking, the supply of fresh fluid may actually be enough to keep the wave-breaking region acting more like an absorber of Rossby wave activity than a reflector.

Figure 5 displays the PV field for a forcing amplitude of 0.1 at three different times during the integration (days 8, 16 and 24, top to bottom), for the Hadley case on the left and the no-Hadley case on the right. As before, we shall concentrate on the low-latitude response. On day 8 the two cases look similar, both having disturbed regions at low latitudes. In the Hadley case this region is further poleward by a few degrees latitude than for the no-Hadley case. This is consistent with linear results

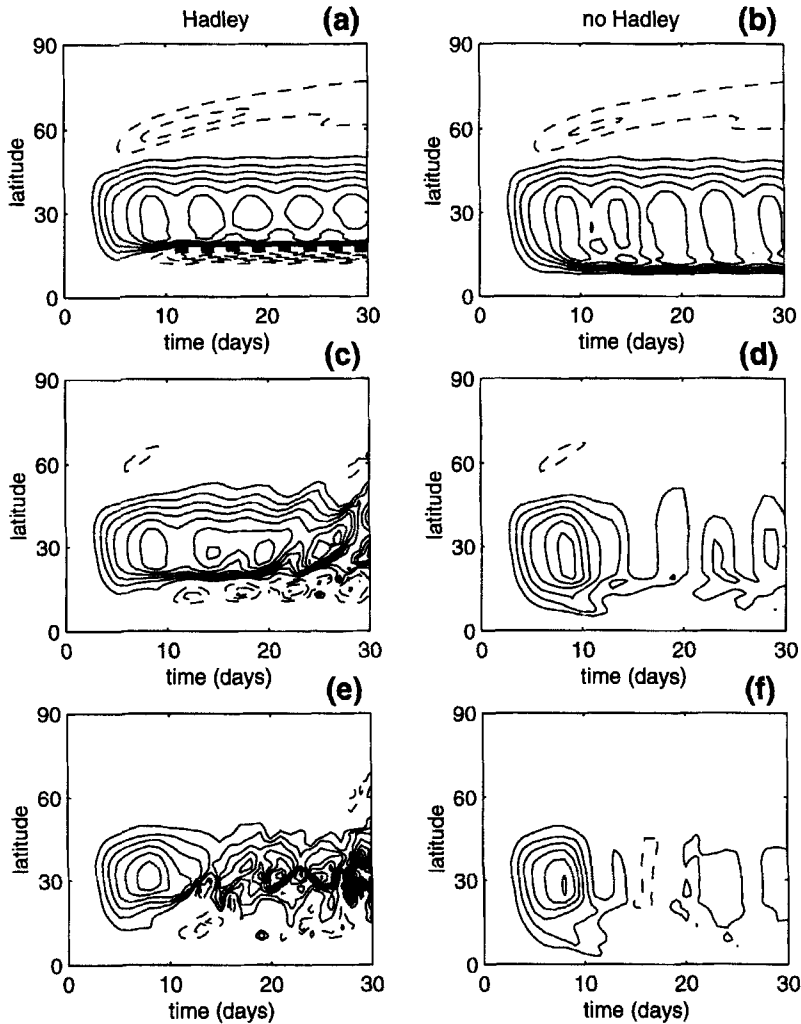


Figure 6. Time evolution (days) of the longitudinal average of the normalized, southward pseudomomentum flux, shown as contour diagrams in the time-latitude plane for wave-number-three forcing of three different forcing amplitudes. Hadley cases are on the left and the no-Hadley cases on the right: (a) and (b) forcing amplitude 0.005; (c) and (d) forcing amplitude 0.05; (e) and (f) forcing amplitude 0.1. Dashed contours are negative.

of the winter Hadley circulation impeding the progress of quasi-stationary planetary waves (e.g. Watterson and Schneider 1987 and references therein). By day 16 the no-Hadley case has developed an almost well-mixed wave-breaking region with isolated PV fragments, but that for the Hadley case is highly disturbed, displaying a wrapped-up PV field. In mid latitudes, in Fig. 5(c), the PV gradient is such that it still supports linear wave propagation, but that is not the case at day 24 of the Hadley case in Fig. 5(e), where the flow has become highly disturbed everywhere in the northern hemisphere. By contrast, the day-24 PV field for the no-Hadley case in Fig. 5(f) still supports linear wave propagation in mid latitudes. We find a similar limit cycle in our experiments as Held and Phillips (1990) describe for finite-amplitude planetary waves interacting

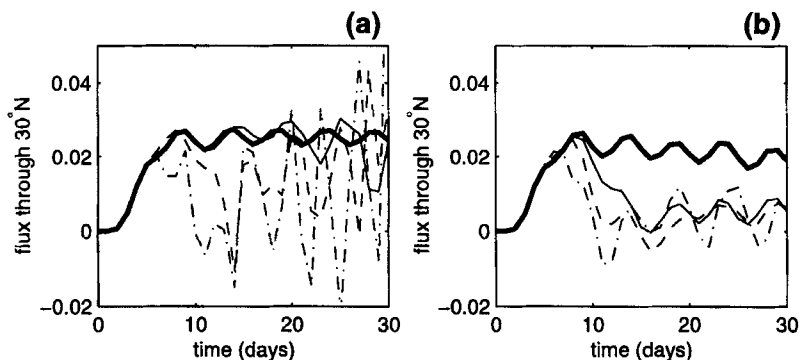


Figure 7. Time evolution (days) of the zonally averaged, normalized, southward pseudomomentum flux through 30°N , with wave number three forcing of amplitudes: 0.005 (thick solid), 0.05 (thin solid), 0.1 (dashed) and 0.2 (dashed-dotted). (a) The Hadley cases, (b) the no-Hadley cases.

with a Hadley cell. Here, we are particularly interested in examining the absorption–reflection behaviour of the wave-breaking region before the mid-latitude PV field gets complicated.

Figure 6 displays contour diagrams of latitudinal distribution and time evolution of the zonally averaged, southward pseudomomentum flux, normalized by the forcing amplitude squared. The diagrams on the left are for the Hadley case, on the right for the no-Hadley case. Figures 6(a) and (b) are for the small-amplitude case of forcing amplitude 0.005. In this instance the low-latitude region is absorptive for all time. The poleward displacement of the wave-breaking region in the Hadley case is clearly visible. Differencing the divergence of the flux for the two cases at small amplitude, reveals that this Hadley experiment leads to a slightly more pronounced displacement of the wave-breaking region than that of EPP. This is consistent with the stronger meridional wind speed in the current Hadley experiments. Another distinct difference between the two small-amplitude cases in Fig. 6(a) and (b) is the poleward pseudomomentum flux that appears at low latitudes in the Hadley case, exactly where pseudomomentum is piling up. This is due to the advective term in the expression for the flux (the first term in (8)), and is not seen in the no-Hadley case. EPP do not show signatures of this advective part in the total flux, because they use a forced basic state for the pseudomomentum calculations such that the advective term is partly cancelled by the term $\sigma_0 v_{\text{Hadley}} u_e \cos \phi$, which also appears on the right-hand side of (8) (as part of S ; v_{Hadley} refers to the meridional wind field in the basic state of EPP, when they force a Hadley cell. In our case $v_{\text{Hadley}} = 0$). The advective part of the flux contributes only over a narrow range of latitudes.

Figures 6(c) and (d) are for a larger amplitude case of 0.05. Here there is a clear indication of reflection for the no-Hadley case (Fig. 6(d)) around day 14; however, there is no such substantial reduction in flux for the Hadley case in Fig. 6(c). For double that forcing amplitude, or 0.1, the reflection occurs earlier, on day 10, for the no-Hadley case. For this amplitude of forcing, even the Hadley case shows some evidence of reflection around day 12, before the flow enters a complicated behaviour.

To ensure that the reduction in flux that is only seen in the highest amplitude Hadley case in Fig. 6 is indeed due to nonlinear reflection, it is convenient to combine several forcing amplitudes on the same diagram. We can do this by looking, for example, at the time evolution of the zonally averaged, southward pseudomomentum flux through a particular latitude (as in MH99). Here we choose to look at 30°N . The results are

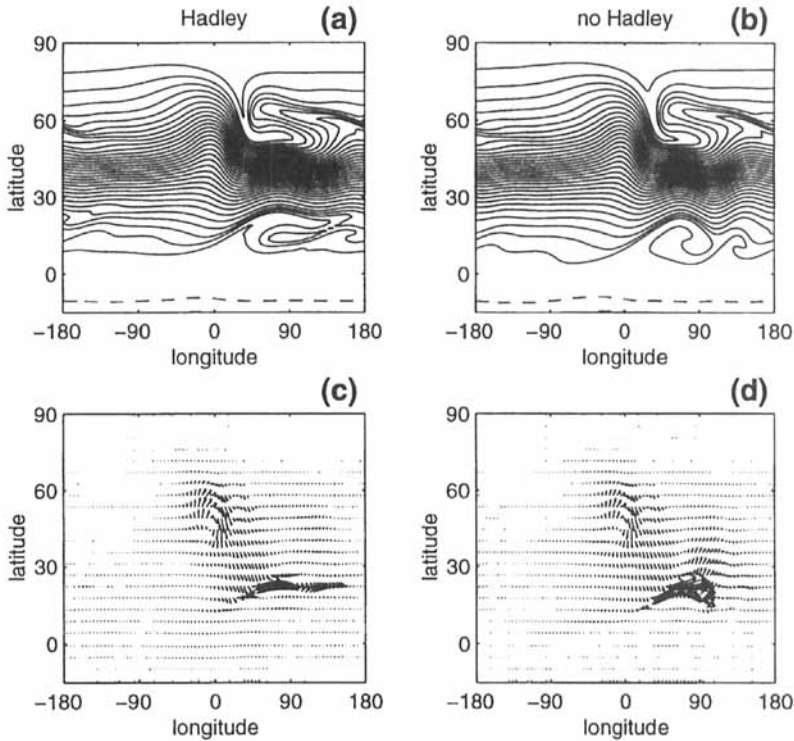


Figure 8. Isolated forcing of amplitude 0.2, 11 days into the simulation. The Hadley case is in the left-hand panels and the no-Hadley case in the right-hand panels. (a) and (b) potential vorticity in the latitude-longitude plane; (c) and (d) pseudomomentum density and flux. Dashed contours are negative.

displayed in Fig. 7(a) for the Hadley case and in Fig. 7(b) for the no-Hadley case. We consider forcing amplitudes 0.005, 0.05, 0.1 and 0.2. For the no-Hadley case, the three strongest forcing amplitudes show a reduction to zero in the flux, with the reduction occurring earlier the stronger the forcing, consistent with signatures of nonlinear reflection. Even the Hadley case shows a reduction in flux to zero, but only for the two strongest forcing amplitudes, and this reduction in flux occurs later than for the corresponding no-Hadley case. We conclude that when the Hadley circulation is active it takes the wave-breaking region longer to get to a reflecting state than when there is no Hadley circulation. By the same token, the minimum wave number three forcing to get to a reflecting state when the Hadley circulation is active is greater than when there is no Hadley circulation. Thus the Hadley circulation delays nonlinear reflection from the wave-breaking region, but it does not prevent it.

(b) *Isolated forcing*

Let us now turn to the more realistic case of an isolated forcing. We placed the Gaussian shaped mountain at 0° longitude and at the same latitude as before (45°N). In addition to the linear forcing amplitude of 0.01, we considered forcing amplitudes of 0.2, 0.3 and 0.4. The response at higher amplitude is displayed in terms of pictures of the PV field and pseudomomentum flux and density. Figure 8 shows such pictures for forcing amplitude 0.2, 11 days into the simulation, for the Hadley case in the left-hand panel and the no-Hadley case in the right-hand panel. As seen in the PV field in Fig. 8(a), at this time there is a gradient of PV in the low-latitude wave-breaking region of the Hadley

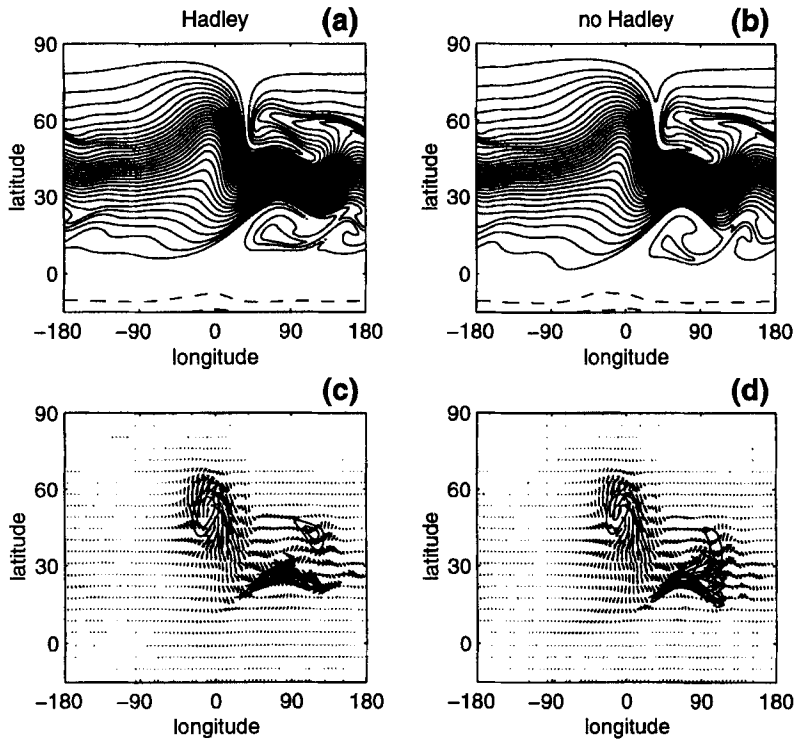


Figure 9. Same as Fig. 8 but for forcing amplitude of 0.4, nine days into the simulation.

case, whereas for the no-Hadley case in Fig. 8(b) the wave-breaking region is already quite mixed. Pseudomomentum has been deposited in the wave-breaking region and, in addition to the flux into that region (that was there in the linear case), there is now a secondary flux of pseudomomentum directed back toward mid latitudes. The return flux is particularly noticeable in the no-Hadley case (Fig. 8(d)) and the flux appears to curve back toward low latitudes around 130°E, consistent with the results of BH for the almost inviscid case. Even when the Hadley circulation is active, a north-east pointing pseudomomentum flux can be seen (Fig. 8(c)) pointing away from the nonlinear wave-breaking region into mid latitudes.

Now, consider double the above forcing. Figure 9 shows pictures similar to those in Fig. 8 except that they correspond to conditions two days earlier in the simulation, on day 9, for forcing amplitude 0.4. Again, the low-latitude PV field is highly disturbed in the wave-breaking region and, even for the Hadley case, there is clearly a pseudomomentum flux directed out of the wave-breaking region and toward mid latitudes. We interpret this result as being a signature of nonlinear reflection.

This conclusion is supported by considering the difference in the meridional component of the velocity (v) between a nonlinear case and a linear case, each normalized by the amplitude of forcing. Figure 10 shows the relevant results, for the Hadley case in the left-hand panel and the no-Hadley case in the right-hand panel, for a forcing amplitude of 0.2 on day 11 at the top, and for forcing amplitude of 0.4 on day 9 at the bottom. Notice the wave train from the wave-breaking region into mid latitudes in each case. The wave trains in the no-Hadley cases are better developed, both for forcing amplitude 0.2 at day 11 (Fig. 10(b)) and for amplitude 0.4 at day 9 (Fig. 10(d)). This is consistent with our

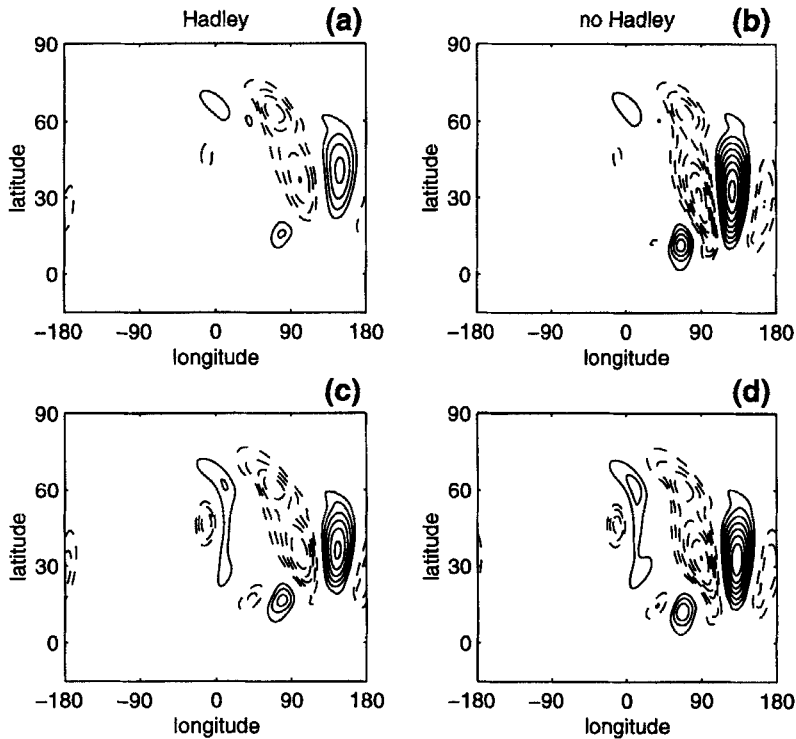


Figure 10. Isolated forcing for Hadley and no-Hadley cases. Latitude–longitude plots of the difference field of latitudinal velocity (Δv) between strongly forced cases and a weakly forced case, each normalized by the forcing amplitude. Hadley cases are on the left, no-Hadley cases are on the right. (a) Δv between an isolated forcing case of amplitude 0.2 and the linear case (amplitude 0.01) on day 11 when the Hadley circulation is active. (b) As (a) except the Hadley circulation is not active. (c) As (a) except for a strong forcing amplitude of 0.4 and on day 9. (d) As (c) except the Hadley circulation is not active. Dashed contours are negative.

previous results for zonally symmetric forcing, that nonlinear reflection is set back when the Hadley cell is active. Furthermore, the no-Hadley reflected wave trains emerge from a lower-latitude location than the corresponding Hadley wave trains. This is consistent with the poleward displacement of the wave-breaking region when the Hadley cell is active that was discussed for the wave-number-three forced case. Thus, the reflected wave trains in the Hadley cases emerge from regions where there is a stronger background zonal flow than is the case with corresponding no-Hadley reflected wave trains. The effects on the reflected wave train may be seen when comparing the left-hand and right-hand panels in Fig. 10, in that the Hadley reflected wave trains are further downstream than the corresponding no-Hadley reflected wave trains. EPP discussed the eastward pseudomomentum flux within the Hadley wave-breaking region due to the strengthened background flow. Careful inspection of the two left-hand panels in Fig. 10 reveals that the reflected wave train in the upper frame (on day 11) is indeed further downstream than the reflected wave train in the lower frame (on day 9). This is consistent with the background flow having had more time to act on the pseudomomentum in the wave-breaking region in the former case. In this context, note that both EPP and the current experiments exaggerate this effect due to the excessively strong jet.

Our conclusion, based on simulations using a SWE model, is that even an isolated wave train can get nonlinearly reflected from a low-latitude wave-breaking region in the presence of a simple representation of a winter Hadley circulation, if the forcing

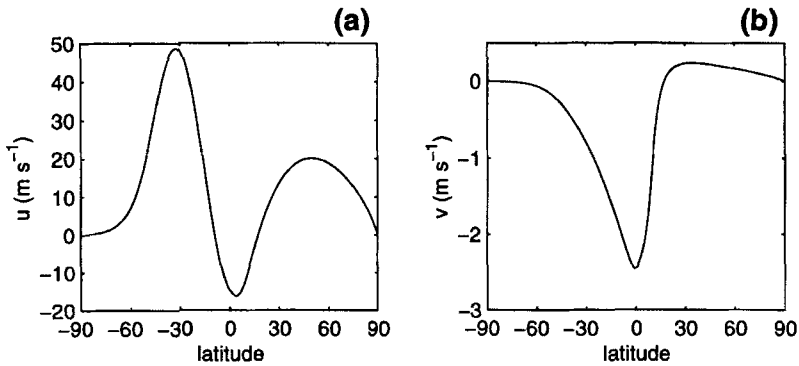


Figure 11. The initial state for the simulations that include a representation of summer Hadley circulation. (a) Zonal wind (m s^{-1}) as a function of latitude; (b) meridional wind in (m s^{-1}) as a function of latitude.

is strong enough. An isolated quasi-stationary wave train is certainly more realistic for tropospheric flows than a wave-number-three wave train.

5. EFFECTS OF A SUMMER HADLEY CIRCULATION ON ROSSBY WAVE PROPAGATION, BREAKING AND REFLECTION

Due to the inherent limitations of the SWE model, it is considerably more difficult to force a summer Hadley circulation than the winter case. Here the mass source was centred at 10°N , everything else was the same as in the winter case. The model was integrated to steady state, and the resulting wind field is shown in Fig. 11. The zonal wind in Fig. 11(a) has easterlies extending to 16°N , which is north of the belt of southward meridional wind speed shown in Fig. 11(b). To circumvent the limitations of the model, we shall consider transient waves of phase speed -10 degrees longitude per day, which corresponds to -12 m s^{-1} at the equator. The critical line of these waves is at 9°N , which is within the belt of cross-equatorial flow. To justify abandoning the stationary waves at this point, suffice it to say that we consider the present steady state with waves of non-zero phase speed to be a substitute for a more realistic steady state with stationary waves superposed on it. The waves were excited by a moving vorticity source of zonal wave number three at 45°N .

Schneider and Watterson (1984) considered the effects of southward flow on the propagation of stationary waves through low-latitude areas of easterly zonal flow in a linear SWE study. They found that flow from north to south allowed linear propagation through layers of negative longitudinal velocity, whereas no such propagation was possible when there was no meridional flow. Based on our experiments in section 3 we would expect, even if such propagation were possible at small amplitude, that as the forcing amplitude is increased such that wave breaking can take place, the free propagation might be prevented.

Figure 12 shows results in terms of the time evolution of the southward pseudo-momentum flux for three different forcing amplitudes. In each case the left panel shows results for the summer Hadley case, and the right panel shows results for the corresponding forcing amplitude when there is no Hadley circulation. As before, the flux is normalized by the forcing amplitude squared. In the small-amplitude case shown in Fig. 12(a) and (b), there is a substantial cross-equatorial flux when the Hadley cell is active, but there is no flux across the critical latitude when there is no meridional flow (Fig. 12(b)). This is entirely consistent with the results of Schneider and Watterson

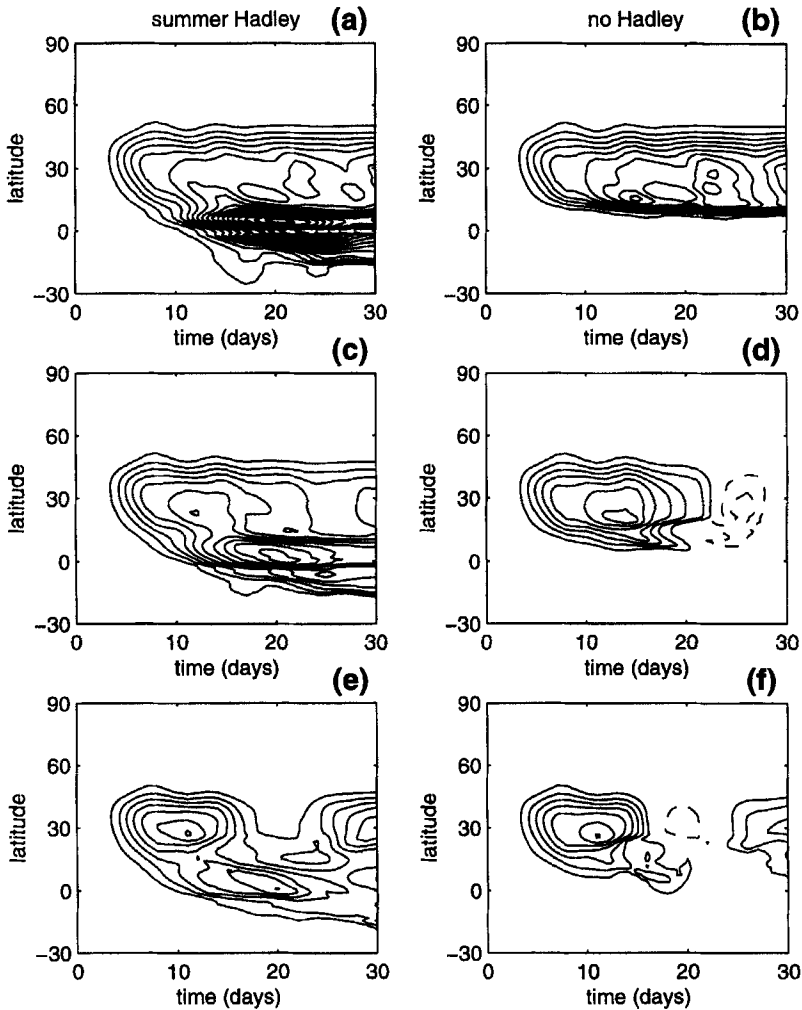


Figure 12. Time evolution (days) of the longitudinal average of the normalized, southward pseudomomentum flux, shown as contour diagrams in the time–latitude plane for wave number three transient forcing of three different forcing amplitudes. Summer Hadley cases are on the left and the no-Hadley cases on the right: (a) and (b) small forcing amplitude; (c) and (d) forcing amplitude 10 times that in (a) and (b); (e) and (f) forcing amplitude 20 times that in (a) and (b). Dashed contours are negative.

(1984). Most of the low-latitude flux in Fig. 12(a) is due to the non-advective part of the flux.

We considered several larger forcing amplitudes. Results for 10 and 20 times the forcing in Fig. 12(a) and (b) are shown in Fig. 12(c) and (d) and Fig. 12(e) and (f), respectively. In both strongly forced cases, the Hadley cell allows for a cross-tropical flux of Rossby wave activity. For the no-Hadley case the flux is abruptly stopped before reaching the critical line, with clear signs of reflection on day 22 in Fig. 12(d) and at day 16 in Fig. 12(f). The Hadley case eventually shows signs of reflection at about day 19 in Fig. 12(e), which is later in the simulation than the corresponding no-Hadley case. For this largest forcing amplitude, both the Hadley and no-Hadley cases show that PV gradients recover through the non-conservative processes, and this allows another build-up of the flux at a later time.

6. CONCLUDING REMARKS

This paper represents further attempts at quantifying the low-latitude absorption–reflection behaviour of quasi-stationary Rossby waves. Rossby wave propagation is the primary mechanism by which longitudinal variations of the time-mean flow are established outside the deep tropics. Reflection from low-latitude wave-breaking regions is, therefore, bound to have pronounced effects on the mid-latitude flow field.

We have shown in numerical simulations, using a SWE model representing the upper troposphere, that quasi-stationary wave trains propagating to low-latitude regions of westerly background wind speed may indeed be reflected back to mid latitudes, provided that the forcing is strong enough. For small-amplitude forcing, the wave train propagates unhindered into the opposite hemisphere. As the forcing is increased, wave breaking takes place, forming a low-latitude surf zone that prevents further linear propagation. When the wave-breaking region saturates, we observe a wave train reflected into the hemisphere of the forcing. One might wonder why we do not detect nonlinear reflection into the opposite hemisphere, considering that the initial state had westerly flow on the equator that could, hypothetically, support wave propagation. After the wave breaking gets established it tends to be most intense on the poleward side of the wave-breaking region while the change in zonal wind tends to be most pronounced on the equatorward side, forming a zero-wind line locally. In fact, an isolated strongly forced wave train can disturb the low-latitude flow field considerably, so that with an easterly initial flow a westerly duct forms just to the west of the wave-breaking region. The details of the formation and evolution of the wave-breaking region, including its evolution when the initial flow field is not axisymmetric, will be the subject of a future paper.

In the same SWE model, now with a weak easterly equatorial background flow, we analysed the behaviour of a wave train in the presence and in the absence of a winter Hadley circulation. The case with no Hadley circulation is similar to the case studied by BH except that we apply Rayleigh friction to the zonally symmetric part of the background flow for direct comparison with the case that includes the Hadley circulation. We found that both a wave-number-three wave train and an isolated wave train may be reflected back to mid latitudes, even in the presence of a Hadley circulation, if the forcing is strong enough. The Hadley circulation leads to a continuous generation of low-latitude PV gradients, so that the wave-breaking region does not become well mixed; still we found strong evidence for reflection back to mid latitudes. Later in the strongly forced simulations, the flow became complicated everywhere such that wave breaking was occurring even in mid latitudes.

In an earlier study MH99 found nonlinear reflection in a simple general circulation model with Newtonian cooling and Rayleigh friction. No attempt was made to simulate the Hadley circulation and only a weak equatorial easterly background flow was considered. Now we have extended this result further, albeit in a SWE model, and found it to apply even in the presence of a simple representation of the Hadley circulation. The result also applies when the background equatorial flow is westerly. We conclude that there is a strong possibility that reflection of tropospheric wave trains from low latitudes may occur in the real atmosphere.

There are several limitations to the present study, the most obvious is the fact that we are using a single-layer model and somewhat idealized basic states that, aside from being longitudinally symmetric, have a PV gradient that is not steep enough in the area surrounding the jet (e.g. Branstator 1983; Hoskins and Ambrizzi 1993). MH99 found in a three-dimensional study that a more realistic initial state, one that had a tropopause sloping in the meridional plane from a high vertical level in low latitudes towards a low vertical level in high latitudes, had a jet that acted more like a longitudinal waveguide

than a state allowing simple latitudinal propagation. Still, the same reflection behaviour was detected in the more realistic basic state (MH99), so that the waveguide was not perfect, allowing some wave activity to seep out to be reflected at low latitudes. This reflection behaviour occurred for forcing amplitudes that resulted in quite reasonable geopotential perturbations at upper levels. In a single-layer model it is difficult to establish the realism of the forcing amplitudes that are applied. However, we believe that the present, rather idealized study is valuable as an intermediate stage on the way to more realistic experiments; these would include more dynamical ingredients that have been omitted so far, but which may be of importance in the real atmosphere. Perhaps the most important feature that has been neglected so far is the interaction of synoptic-scale eddies with the large-scale waves that are the focus of this study. Such issues may be resolved by controlled experiments using general circulation models that, in addition to synoptic eddies, include physical processes which may be of importance for the reflection-absorption behaviour of the real atmosphere.

ACKNOWLEDGEMENTS

The authors thank Darryn Waugh for helpful comments. This work was supported by NSF Grants ATM-9615864 and ATM-9908883.

REFERENCES

- | | | |
|---------------------------------------------------|------|---------------------------------------------------------------------------------------------------------------------------------------------------------------------------------|
| Branstator, G. | 1983 | Horizontal energy propagation in a barotropic atmosphere with meridional and zonal structure. <i>J. Atmos. Sci.</i> , 40 , 1689–1708 |
| | 1992 | The maintenance of low-frequency atmospheric anomalies. <i>J. Atmos. Sci.</i> , 49 , 1924–1945 |
| Brunet, G. and Haynes, P. H. | 1996 | Low-latitude reflection of Rossby wave trains. <i>J. Atmos. Sci.</i> , 53 , 482–496 |
| Edmon, H. J., Hoskins, B. J. and McIntyre, M. E. | 1980 | Eliassen–Palm cross-sections for the troposphere. <i>J. Atmos. Sci.</i> , 37 , 2600–2616 |
| Esler, J. G., Polvani, L. M. and Plumb, R. A. | 2000 | The effect of the Hadley circulation on the propagation and reflection of planetary waves in a simple one-layer model. <i>J. Atmos. Sci.</i> , 57 , 1536–1556 |
| Fulton, S. R. and Schubert, W. H. | 1985 | Vertical normal mode transforms: Theory and application. <i>Mon. Weather Rev.</i> , 113 , 647–658 |
| Grose, W. L. and Hoskins, B. J. | 1979 | On the influence of orography on the large-scale atmospheric flow. <i>J. Atmos. Sci.</i> , 36 , 223–234 |
| Haynes, P. H. | 1988 | Forced, dissipative generalizations of finite-amplitude wave-activity conservation relations for zonal and non-zonal basic flows. <i>J. Atmos. Sci.</i> , 45 , 2352–2362 |
| Held, I. M. | 1985 | Pseudomomentum and the orthogonality of modes in shear flows. <i>J. Atmos. Sci.</i> , 42 , 2280–2288 |
| Held, I. M. and Phillips, P. J. | 1990 | A barotropic model of the interaction between the Hadley cell and a Rossby wave. <i>J. Atmos. Sci.</i> , 47 , 856–869 |
| Hoskins, B. J. and Ambrizzi, T. | 1993 | Rossby wave propagation on a realistic longitudinally varying flow. <i>J. Atmos. Sci.</i> , 50 , 1661–1671 |
| Hoskins, B. J. and Simmons, A. J. | 1975 | A multi-layer spectral model and the semi-implicit method. <i>Q. J. R. Meteorol. Soc.</i> , 101 , 637–655 |
| Hoskins, B. J., Simmons, A. J. and Andrews, D. G. | 1977 | Energy dispersion in a barotropic atmosphere. <i>Q. J. R. Meteorol. Soc.</i> , 103 , 553–567 |
| Hsu, H.-H., Hoskins, B. J. and Jin, F.-F. | 1990 | The 1985/86 intraseasonal oscillation and the role of the extratropics. <i>J. Atmos. Sci.</i> , 47 , 823–839 |
| Kiladis, G. N. and Weickmann, K. M. | 1992 | Extratropical forcing of tropical Pacific convection during northern winter. <i>Mon. Weather Rev.</i> , 120 , 1924–1938 |
| Killworth, P. D. and McIntyre, M. E. | 1985 | Do Rossby-wave critical layers absorb, reflect or over-reflect? <i>J. Fluid Mech.</i> , 161 , 449–492 |
| Magnusdottir, G. and Haynes, P. H. | 1996 | Wave-activity diagnostics applied to baroclinic-wave life cycles. <i>J. Atmos. Sci.</i> , 53 , 2317–2353 |
| | 1999 | Reflection of planetary waves in three-dimensional tropospheric flows. <i>J. Atmos. Sci.</i> , 56 , 652–670 |

- Min, W. and Schubert, S. D. 1997 'Interannual variability and potential predictability in reanalysis products'. NASA Technical report, NASA/TM-97-104606, Vol. 13
- Plumb, R. A. 1985 On the three-dimensional propagation of stationary waves. *J. Atmos. Sci.*, **42**, 217–229
- Schneider, E. K. and Watterson, I. G. 1984 Stationary Rossby wave propagation through easterly layers. *J. Atmos. Sci.*, **41**, 2069–2083
- Vanneste, J. and Shepherd, T. G. 1998 On the group-velocity property for wave-activity conservation laws. *J. Atmos. Sci.*, **55**, 1063–1068
- Waugh, D. W., Polvani, L. M. and Plumb, R. A. 1994 Nonlinear barotropic response to a localized topographic forcing: Formation of a 'tropical surf zone' and its effect on inter-hemispheric propagation. *J. Atmos. Sci.*, **51**, 1401–1416
- Watterson, I. G. and Schneider, E. K. 1987 The effect of the Hadley circulation on the meridional propagation of stationary waves. *Q. J. R. Meteorol. Soc.*, **113**, 779–813
- Webster, P. J. and Holton, J. R. 1982 Cross-equatorial response to middle latitude forcing in zonally varying basic state. *J. Atmos. Sci.*, **39**, 722–733